H-mode and Non-Solenoidal Startup in the Pegasus Ultralow-A Tokamak

R.J. Fonck[1], J.L. Barr[1], G. M. Bodner[1], M.W. Bongard[1], M.G. Burke[1], D. M. Kriete[1], J.M. Perry[1], J.A. Reusch[1], D.J. Schlossberg[1], C.R. Sovinec[1], and K. E. Thome[1,2]

[1]University of Wisconsin-Madison, Madison, WI, USA

[2]Oak Ridge Associated Universities, Oak Ridge, TN, USA

E-mail contact of main author: rjfonck@wisc.edu

Abstract. Studies at near-unity aspect ratio offer unique insights into advanced tokamak physics and support development of novel startup scenarios. Ohmic H-mode operation has been attained at $A < 1.3$. Unlike at high A, P_{LH} is comparable in limited and single-null diverted topologies at $A \sim 1.2$, consistent with the theoretical FM3 model predictions. The magnitude of P_{LH} exceeds ITPA scalings by an order of magnitude, with P_{LH}/P_{ITPA08} increasing as A approaches 1. $J_{edge}(R,t)$ measurements across single ELMs show the nonlinear generation and expulsion of current-carrying filaments during the ELM crash. Helical edge current injection appears to mitigate Type III ELM activity. Localized current injection at the plasma edge provides a scalable means of injecting DC helicity for initiating and possibly driving tokamak current. $I_p \sim 0.18$ MA has been initiated without an Ohmic solenoid, and initial measurements show T_e and pressure profiles that are comparable to Ohmically driven plasmas. Resistive MHD simulations and supporting observations suggest I_p is built from current rings injected during reconnection between unstable helical current streams. This noninductive startup technique allows production of stable plasmas with very high toroidal field utilization, $I_p/I_{TF} > 2$ and normalized current $I_N > 12$. The magnetic reconnection activity inherent in this process provides an auxiliary ion heating mechanism that may facilitate access to high β_T values.

1. Introduction

Some perhaps underappreciated consequences of operation at ultra-low aspect ratio $A \leq 1.2$ are: ready access to the H-mode confinement regime; natural elongation and triangularity; strong peeling and ballooning instability drive to excite Edge Localized Modes (ELM); potential operation in low collisionality regimes with neoclassical effects; and ready access to plasmas with very high toroidal beta. These features are attained even at modest scale and temperatures, where detailed internal probe measurements of the local current density and pressure with high spatiotemporal resolution are possible.

In the Pegasus ultra-low aspect ratio tokamak [1], these unique properties of operation at near-unity aspect ratio are exploited to perform experiments that complement those at larger scale. Pegasus is a university-scale ($R \sim 0.4$ m, $a \sim .35$ m, $I_p \leq 0.3$MA, $B_T \leq 0.15$T) experimental component of the US national spherical tokamak program. It accesses $A \sim 1$ in the tokamak-spheromak transition region, which naturally leads to large values of the normalized plasma current, $I_N = I_p/aB_T$, or equivalently the toroidal field utilization factor I_p/I_{TF} ($I_N = 5AI_p/I_{TF}$). Plasmas with $A \geq 1.13$ are produced in Pegasus using a novel high-stress solenoid magnet assembly ($B_{sol} \leq 15$ T) and with localized DC helicity injection coupled to subsequent Ohmic induction.

Local Helicity Injection (LHI) is being developed on the Pegasus experiment for non-solenoidal plasma startup and current drive. In LHI, strong localized electron currents injected along the magnetic field lines in the plasma edge region relax through helicity-conserving magnetic turbulence to form a tokamak-like plasma. $I_p \sim 0.18$ MA has been attained with $I_{inj} \sim$

6 kA to date, and the technique holds promise for extension to larger-scale tokamaks. Coincidentally, these plasmas can access stable operation at very high normalized current $I_N > 12$ while providing auxiliary reconnection-driven ion heating to produce spherical tokamak plasmas with a potential for high toroidal beta.

2. H-mode and Edge Stability Studies

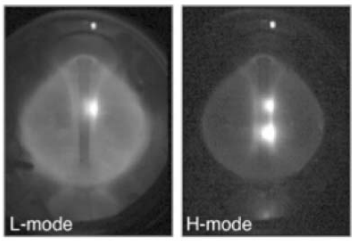
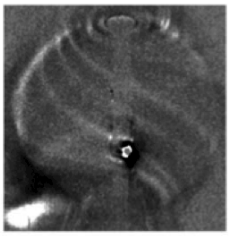


Fig. 1. Fast images of diverted plasmas.

The naturally low B_T needed for stability at $A \leq 1.2$ reduces the L- H mode power threshold, P_{LH}, so that H-mode plasmas are achieved with Ohmic heating alone in both limited and diverted magnetic topologies [2]. H-mode plasmas were attained at near-unity $A \sim 1.2$ in Pegasus with Ohmic heating following the installation of a high-field-side neutral fueling system. Characteristic signatures of H-mode access with an L-H transition include a marked reduction in D_α line radiation compared to L-mode plasmas, punctuated by sharp bursts from ELMs. A bifurcation in diamagnetic flux ϕ_D occurs at the transition. Equilibrium reconstructions indicate a doubling of τ_E following this transition time.

Initial H-mode studies were performed in inner-wall limited magnetic topology. After installation of new divertor coils, diverted L- and H-mode plasmas are now attainable (Fig. 1). The operating space in diverted plasmas is constrained by the short pulse and limited V-s of the present facility; negative V_{loop} is induced by the rapid variations in the divertor field. Upgrades to the KFIT equilibrium code [3,4] were enacted to accurately model the induced wall currents in the X-point region. This includes a finite-coil solution grid domain and accurate calculation of Green response functions at $A \sim 1$ [5,6].


Fig. 2. ELM filaments.

Access to ELMs is readily achieved in H-mode operation. Figure 2 shows a fast visible image of an ELM in Pegasus. As on other devices [7], 3D field-aligned filaments are generated, along with bursty D_α emission on ~100 μs timescales. Irregularly-spaced filaments are commonly observed, indicating nonlinear interaction of edge peeling-ballooning modes [8,9,10].

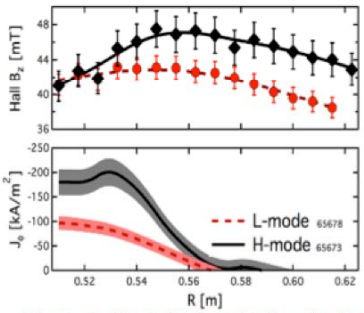


Fig. 3. $B_Z(R)$, $J_\phi(R)$ from Hall probe [10].

Radially-scanning probes are tolerated through the pedestal without measurable plasma perturbation. Figure 3 shows J_{edge} profiles measured with a multichannel Hall probe array [2]. Multi-shot radial scans of a triple Langmuir probe (Fig. 4) indicate electron pressure pedestal formation as well, consistent with a conventional hyperbolic tangent pedestal model [11]; however, this initial $p_e(R)$ scan was complicated by edge distortion from strong internal $n = 1$ internal tearing mode activity.

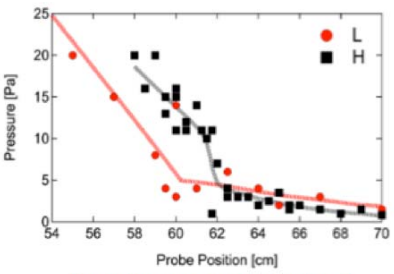


Fig. 4. H-mode pressure pedestal.

Measured P_{LH} exceeds predictions from accepted international scalings [12] by an order of magnitude or more. Figure 5 shows Pegasus results in comparison with published L-H P_{LH} from an ITPA database from a variety of machines [12,13,14]. The P_{LH}/P_{ITPA08} scaling law discrepancy significantly increases as $A \to 1$, confirming a trend suggested by NSTX and MAST. Nonetheless, P_{LH} increases with n_e, consistent with the ITPA08 scaling law (cf. Fig. 6 for inner-wall limited and favorable ∇B single-null

discharges). These studies did not detect a P_{LH}-minimizing density [15]. Another unique feature observed at low-A was that the L-H power threshold is, to date, insensitive to magnetic topology (i.e., limited vs. diverted). Similar comparisons at conventional $A \sim 3$ indicate that $P_{LH}^{LIM}/P_{LH}^{DIV} \sim 1.5$–$3$.

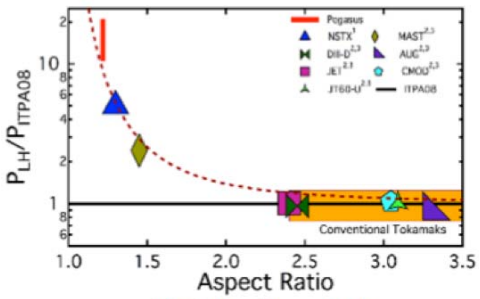


Fig. 5. P_{LH} / P_{ITPA08} vs. A.

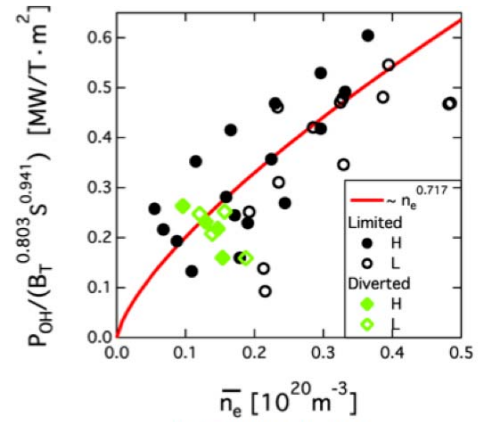


Fig. 6. H-mode P_{OH} vs. n_e.

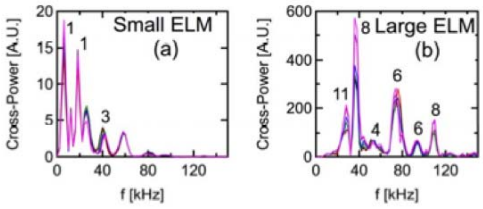


Fig. 7. Measured ELM toroidal mode numbers.

Both of these observations are consistent with the FM3 L-H transition model [16]. The $P_{LH}^{LIM}/P_{LH}^{DIV}$ value is proportional to the ratio of edge q_ψ in limited and diverted topologies. In Pegasus, the A~1 geometry virtually eliminates the difference in q_ψ between the topologies, in contrast to high-A behavior. The magnitude of P_{LH} is not consistent with FM3, which replicates the ITPA08 scaling by construction.

Two classes of ELMs have been identified to date, with differing toroidal n distributions (Fig. 7). Small, Type III-like ELMs occur at input power $P_{OH} \sim P_{LH}$ and show low-n (≤ 4) magnetic signatures via a radially-scanning Mirnov coil array [17]. At $P_{OH} \gg P_{LH}$, ELMs transition to larger Type I-like, with intermediate $5 < n < 15$ being dominant and increased per-ELM energy losses.

While Type I ELMs are universally found to be intermediate n, the dominant Type I-like ELM mode numbers in both Pegasus and NSTX [18] are lower than those typical on higher-A devices [34]. Type III-like ELMs exhibit a different relative n relationship with respect to Type I ELMs as A is varied. In Pegasus and NSTX [18], Type III n are lower than Type I, while at higher A, n increases instead [19]. These differences are attributed to the naturally high J_{edge}/B peeling mode drive arising at low A [11,21,22].

The low-n magnetic spectra of Type III ELMs are similar to those measured during the nonlinear evolution of the peeling mode alone. Studies on Pegasus found the peeling mode generates ELM-like filaments (Fig. 8(a), [21]). It has a high-m, low-n and edge localization consistent with an external kink, which was found to be unstable in DCON stability analyses of those discharges (Fig. 8(b), [17]).

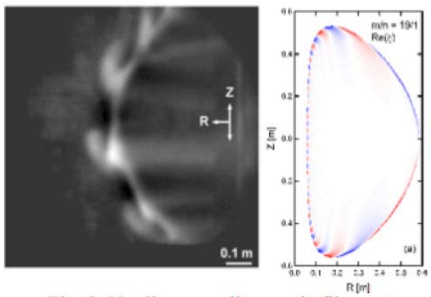


Fig. 8. Nonlinear peeling mode filaments [11], mode displacement [12].

Both small and large ELMs, separated by a brief ELM-free period are observed in a single discharge as I_p and the heating power P_{OH} is ramped. After a strong P_{OH} ramp, an ELM-free period can be terminated by a large, disruptive Type I ELM. As seen elsewhere, this Type I ELM leads to spiral energy deposition patterns on the divertor regions. Both ELM types create filament bursts, such as in Fig. 3-3; however, this strike point illumination represents a unique indicator of Type I ELMs in the experiment.

Nonlinear ELM dynamics have been observed in Pegasus. Figure 9 shows the evolution of a dominant $n = 8$ and sub-dominant $n = 6$ modes on Mirnov dB_Z/dt signals during a Type

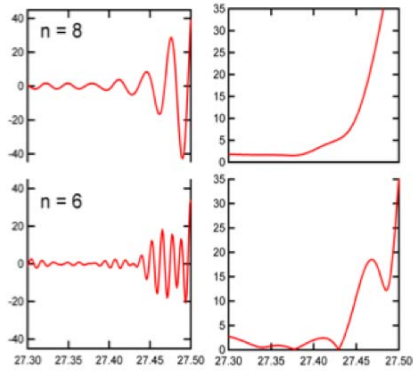


Fig. 9. Nonlinear evolution of n = 8,6 mode magnetic amplitudes in Large ELM crash.

I ELM crash. The $n = 8$ mode grows exponentially, whereas the $n = 6$ mode exhibits a more complex growth and decay pattern. These data are consistent with the theoretical expectation of instability to a spectrum of n during an ELM, and are in qualitative agreement with nonlinear simulations demonstrating nonlinear coupling, growth, and decay of competing sub-dominant toroidal harmonics.

Unique measurements of the edge current density profile and its dynamics have been attained through a single ELM cycle. Figure 10 shows the complex evolution of $J_{edge}(R, t)$ during a large ELM crash. From its pre-ELM value, the edge current density builds over ~100 μs. The peak J_{edge} transiently relaxes to an L-like, wider pedestal gradient, followed by the formation and ejection of a current filament that accelerates from the post-ELM edge. The inferred filament generation is temporally coincident with an outwardly propagating filament observed via visible imaging. Filament ejection by nonlinear peeling-ballooning modes is hypothesized by electromagnetic blob transport theory [22], observed in nonlinear ELM simulation [23], and is qualitatively similar to prior experimental studies of the nonlinear peeling mode on Pegasus [21].

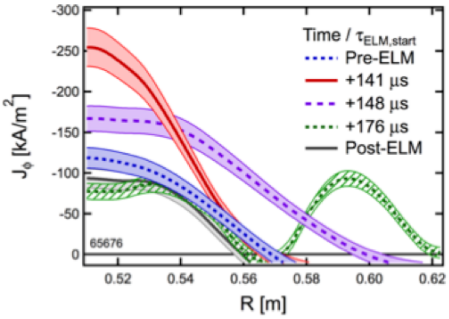


Fig. 10. $J_{edge}(R)$ dynamics, filament election in Type I ELM..

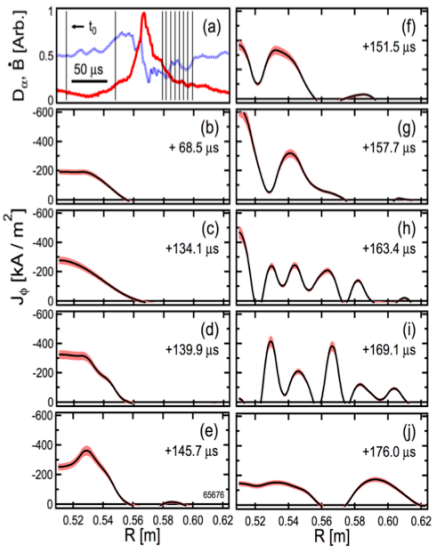


Fig. 11. Type I ELM nonlinear $J_{edge}(R,t)$ evolution.

A more detailed view of these data employing less spatial averaging reveals more complicated dynamical behavior on Alfvénic time scales (Fig. 11). Time values are referenced to the first detectable rise in ELM magnetic activity, ~75 μs prior to the rise in D_α signal [Fig. 11(a)]. The pre-ELM current pedestal builds over ~135 μs [Fig. 11(b)–(d)]. During the following ~40 μs collapse phase [Fig. 3-15(e)–(l)], J_{edge} first develops fragmentary "current-hole" perturbations [Fig. 11(e)–(f)] that expand past the equilibrium last closed flux surface at $R \approx 0.56$ m [Fig. 11(g)]. Current is transported radially outward, transiently relaxing through a wider pedestal gradient [Fig. 11(h)]. J_ϕ then coalesces into two regions separated at $R \approx 0.57$ m that become the post-ELM pedestal and a current-carrying filament [Fig. 11(i)–(k)]. The filament is subsequently expelled and radially accelerates away from the plasma [Fig. 11(l)].

These are the first such measurements during an ELM cycle, and—combined with detailed measurements of the time-evolving pressure in the future—these measurements can provide unique experimental tests of nonlinear models of ELM evolution.

Leveraging the edge current injectors normally used for LHI, but at lower power, may afford a novel means of ELM modification through helical edge magnetic perturbations. Figure 12 shows initial investigations of the effects of injecting perturbing helical current streams several cm outside the edge pedestal along open field lines in the scrapeoff layer adjoining a

H-mode plasma. This is conceptually similar to experiments conducted on EAST, where the helical edge current injection was established via RF current drive instead of helicity injectors. At relatively low $I_{inj} \leq 1$ kA, no effects on I_p or Φ_D are evident [Fig. 12(a)]. However, a marked decrease in small, Type III-like ELM activity occurs, as illustrated by reduced high-frequency D_α bursts in Fig. 12 (b),(c). For $I_{inj} > 2$ kA, a strong drop in I_p is evident as increasing perturbing field is applied, consistent with very strong perturbations of the edge and loss of H-mode confinement. These proof-of-principle experiments may be extended in future work.

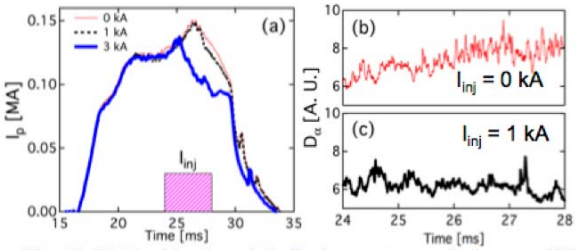


Fig. 12. ELM mitigation via helical current perturbation: small ELMs - sharp spikes in D_α signal in (b) - suppressed with I_{inj} = 1kA (c).

3. Non-solenoidal Startup via Local Helicity Injection

A 0-D power balance model for $I_p(t)$, using helicity conservation and Taylor limits, has been formulated to provide a predictive description of $I_p(t)$ during LHI drive from initiation of the discharge to termination of the helicity drive. Given a position and shape trajectory of the plasma and an estimate of the plasma resistivity, the measured $I_p(t)$ is reasonably well-described, as shown in Fig. 13(a). The model also shows that helicity-driven effective loop voltage, V_{eff}, is dominant early in the evolution, with inductive contributions from changing plasma shape and inductance, and poloidal field induction dominating later in the discharge [Fig. 13(b)].

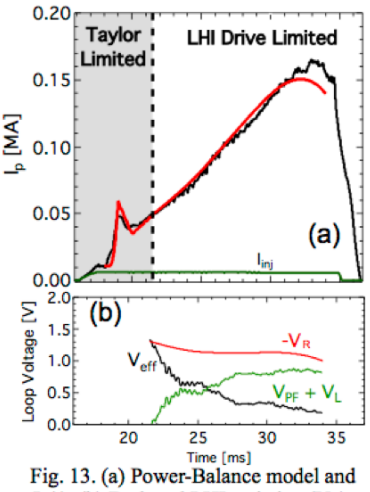


Fig. 13. (a) Power-Balance model and $I_p(t)$. (b) Deduced LHI resistive (V_R), Helicity-driven (V_{eff}), and inductive ($V_{PF} + V_L$) drive voltages.

Since the effective drive voltages are mainly inductive during much of the discharge, the evolution of $I_p(t)$ is somewhat controlled by simply programming the evolution of the plasma shape. This is seen in Fig. 14, where different evolutions of $I_p(t)$ are predicted by the 0-D model for varied evolutions of the plasma major radius and associated plasma shape. The attained $I_p(t)$ follows the modeled values reasonably well. While useful in guiding further LHI investigations, this model presently suffers from no predictive knowledge of the electron temperature or its expected scalings.

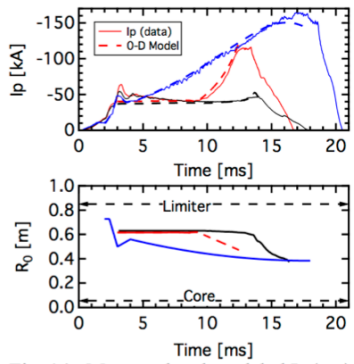


Fig. 14. Measured and modeled I_p (top) for varied plasma geometry evolution (bottom)..

I_p increases with increased helicity input when I_p falls below the Taylor limit. This supports the expectation of higher current as the helicity input is raised with high-field-side divertor injectors ($V_{eff} \sim V_{inj}A_{inj}B_{TF}$). Parametric dependencies of the Taylor-limited I_p on B_T and I_{inj} were confirmed [24]. The Taylor limit is absolute: addition of Ohmic loop voltage during LHI does not increase I_p above the Taylor limit in these driven plasmas, in contrast to Ohmic plasma behavior. Confirmation of the Taylor limit allows confident specification of current injector parameters for new LHI deployments.

A dramatic collapse of V_{inj} to $\leq$ 500V associated with cathode spot ignition on the injector anode can result in a catastrophic loss of helicity current drive (i.e., V_{eff}). A multi-year

development effort has produced high-J, high-voltage current injectors that can reside next to the tokamak last closed flux surface without deleterious PMI. Conversion of the high-V_{inj} arc anode/bias cathode convex frustum shape minimizes the deleterious effects of cathode spot breakdown [25] by steering them away from insulating injector components and thereby avoiding impurity generation and core plasma pollution. A set of electrically isolated shield rings minimize the likelihood of igniting cathode spots and reverse-current breakdown by reducing the local electric field concentration on any given surface. These improvements enable attainment of $V_{inj} \sim 1.5$ kV for fully conditioned injectors.

LHI startup has been demonstrated to successfully initiate a target plasma that transitions to H-mode in the subsequent OH-driven phase. This increases the net available V-s and produces high-I_p targets that are compatible with rapid transition to H-mode (Fig. 15). The highest I_p H-modes in the device have been produced with this technique, in part due to a favorably broad J(R) from LHI startup stabilizing $n = 1$ tearing modes that otherwise degrade OH plasmas with limited V-s.

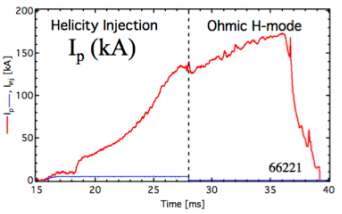


Fig. 15. LHI → OH H-mode startup.

A multipoint Thomson scattering system was installed and brought into operation [26-28]. Thomson scattering spectra have been attained in the core region of high density L-mode plasmas, with central $T_e \sim 150$ eV. A multi-shot, spatially averaged Thomson scattering spectrum consistent with core $T_e(0) \sim 75$-100 eV was obtained during LHI.

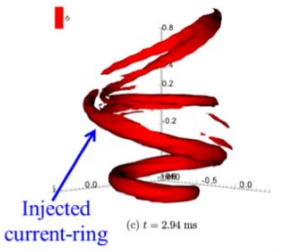


Fig. 16. Reconnecting current streams in NIMROD [33].

Nonlinear MHD modeling of the LHI startup process with NIMROD [29] indicates that the injector-driven current streams are persistent during LHI. The tokamak-like plasma is built up from axisymmetric rings of plasma that are formed by reconnection between adjacent turns of the driven current streams (Fig. 16, [30]) that also produce bursty MHD activity. Experimental signatures qualitatively consistent with this paradigm have been observed. Either continuous or bursty $n = 1$ activity is always observed as I_p evolves during LHI [31]. Typical MHD bursts show coherent signals between detectors in toroidal and poloidal Mirnov coil arrays on the outer low-field side of the facility.

Modeling the predicted unstable current streams as a rotating kink-deformed stream allows pairwise coherence analysis to infer the location of the stream location region to be near the midplane region at the injector major radius. Fast visible imaging has occasionally detected axisymmetric rings early in LHI startup. Hall probe measurements of coherent $n = 1$ MHD spatially localize the activity to a region centered about the major radius of the helicity injectors (Fig. 17). Figure 18 compares experimental I_p, Mirnov coil fluctuations, and a spectrogram of MHD activity with comparable synthetic diagnostics applied to NIMROD simulation output [32]. Finally, strong anisotropic ion heating is observed in the plasma edge region, consistent with the location of the reconnecting current streams. These preliminary comparisons to NIMROD motivate plans to directly detect the dynamic, reconnecting current streams.

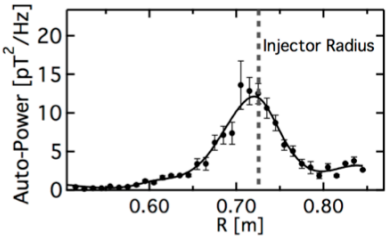


Fig. 17. n=1 MHD activity during LHI localized to injector radius.

The LHI results discussed above focus exclusively on the case where the currents injectors were located near the outer low-field-side midplane of the driven tokamak-like plasma. These plasmas were driven in the high-I_p phase of the discharge by inductive voltage arising from

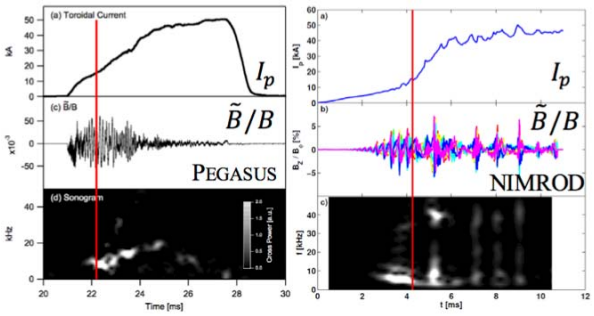


Fig. 18 Comparison of $I_p(t)$ and magnetic fluctuations signals for experiment (left) and NIMROD simulation (right).

the strongly time-varying plasma geometry. Extrapolation of this startup technique to larger scale requires study of LHI startup when the majority of the effective drive voltage is derived from the helicity input. To that end, two relatively large-area injectors have been installed in the lower divertor region, similar to the early small injector tests reported by Eideitis et al. [33] This new configuration allows startup of a toroidal plasma at lower major radius, which significantly decreases the amount of inductive volt-seconds, while increasing the V_{eff} by ~3x due to a 3-fold reduction in the major radius of the injectors.

Relaxation to the tokamak state is achieved in this geometry by aggressive shaping of the vacuum poloidal field structure. This simultaneously strengthens B_z in the injector region (to enable injection without one current stream impacting the opposite injector) and weakens it near the midplane region so that the induced field can overwhelm the vacuum B_z. While I_p ~ 0.1 MA has already been achieved with this divertor injector configuration, operation at full B_T is limited to date by increased plasma-material interactions and the onset of large cathode spots leading to transient loss of V_{eff} as I_p rises. This increased PMI as B_T increases appears to be due to misalignment of the injectors with the local field line pitch.

4. Access to High β_T with Non-Solenoidal Current Drive

Operation with divertor injectors at lower B_T to avoid this deleterious PMI allows access to $I_p \leq 0.15$ MA with $I_p/I_{TF} > 2$. This provides $I_N > 12$, a factor of two or more higher than previously achieved in ST experiments. This in principle may provide access to tokamak plasmas with unprecedentedly high β_T values in a high I_p discharge with no ohmic drive. Sample waveforms for a plasma with I_p/I_{TF} ~1.8 using purely LHI drive to a nominal flattop current are shown in Fig. 19. Assuming minimal 3-D effects due to the current stream injection in the edge region, magnetic equilibrium reconstructions suggest $\beta_T \geq 0.4$ for these discharges when the toroidal field is held constant and possibly higher when the B_T is ramped down during the discharge to I_p/I_{TF} ~ 2.4. Here β_T is defined by the conventional $\beta_T = 2\mu_0\langle p\rangle/B_{T0}^2$ where B_{T0} is the vacuum toroidal field at the plasma major radius. However, this data is preliminary in that the magnetic analyses have not yet been confirmed with kinetic measurements of the plasma temperatures and densities. The ultimate stability limits have not yet been established. Some discharges end in disruption with a low-n precursor mode, while others are limited by pulse length.

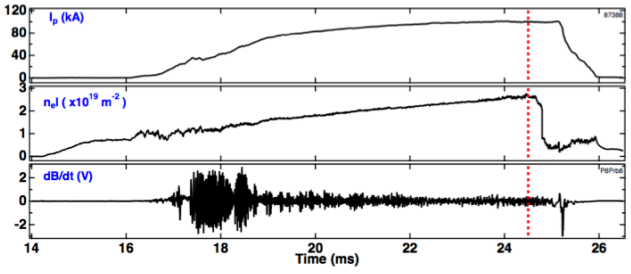


Fig. 19. Current, density, and magnetic activity for divertor injection discharge.

Simple ohmic heating of the electrons is typically insufficient to supply enough stored energy for high β_T operation. However, the magnetic reconnection activity associated with the LHI current drive process has been observed to significantly heat the plasma ions, as indicated in impurity ion temperature measurements for both LHI and OH driven plasmas phases (Fig. 20). The measured impurity ion temperature is typically 1-3 times $T_e(0)$ in plasmas generated by LHI. Tests of ion heating due to current stream reconnection without a tokamak plasma present shows anisotropic heating that scales with v_{Alfven}^2 in agreement with two-fluid reconnection theory (c.f. Fig. 21). Hence, the reconnection–driven anomalous ion heating could provide a key auxiliary ion heating needed to access a high β_T regime. Manipulation of this current-stream driven reconnection ion heating may provide an independent control actuator for exploring this high β_T regime in future experiments.

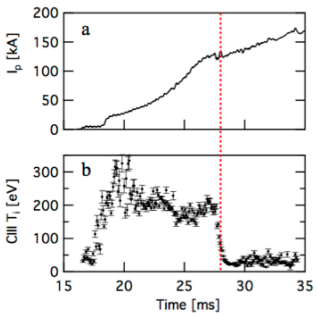


Fig. 20. $I_p(t)$ and $T_{i,CIII}(t)$ for LHI and OH (H-mode) plasmas

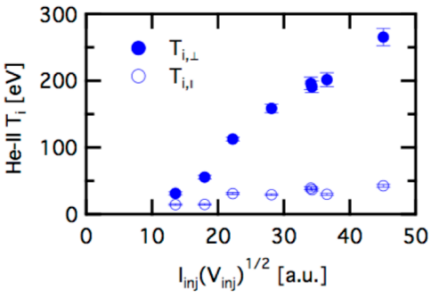


Fig. 21. Inhomogeneous ion heating due to reconnection between injected current streams. The abscissa is proportional to v_{Alfven}^2.

5. Discussion

The Local Helciity Injection approach to plasma startup and growth appears to scale to larger experiments such as NSTX-U and beyond. The development of injector technology that can perform adequately in the near scrapeoff region is a challenge comparable to developing the physical understanding of the processes active in this 3-D current system. In the near term, the emphasis of future studies will concentrate on extending studies of helicity injection for plasma startup, and possibly as a tool for manipulating the edge of fully established high current plasmas in large facilities. A main focus is on demonstrating an approach that can provide ~ 1 MA startup on the NSTX-U experiment. To that end, a simple coaxial helicity injection capability is under consideration to compare and contrast the coaxial and local injection approaches. Determining a predictive model or scaling for the electron energy confinement is especially important since the plasma resistivity determines the helicity dissipation rate and hence directly controls the current drive efficiency.

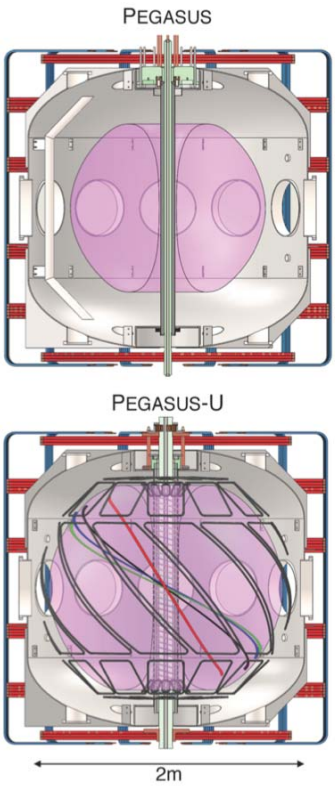


Fig. 22. Cross sections of Pegasus (top) and conceptual Pegasus-U (bottom).

The non-inductive startup afforded by helicity injection allows access to high-I_p plasmas at very low B_{TF}, which in turn offer the opportunity to study very high β_T plasma with relatively modest experimental capabilities. This will also be a focus of study as the startup techniques are refined.

The results to date on H-mode transition properties and ELM dynamics demonstrate the potential for detailed fusion science studies in support of larger experiments by operating at very low A and modest scale. Similarities and differences in H-mode transition and ELM properties have already been observed. More importantly, operation at the very low B_{TF}

afforded by low-A facilitates the use for simple probes for internal measurements of the plasma dynamics during transient events such as ELMs with high spatiotemporal resolution.

In the longer term, relatively modest upgrades to the experimental facility are under consideration to enable further studies of the H-mode and ELM dynamics (Fig. 22). A larger solenoid and new TF center-rod assembly would provide high I_p operation and longer pulse to achieve transport equilibrium and observe multiple large ELM events. Upgraded OH and TF power systems can support this operation at $A \approx 1.25$, which is sufficiently low to provide H-mode access with only Ohmic heating. An extensive 7 (poloidal) x 12 (toroidal) 3D Magnetic Perturbation coil system, plus a 4-in-hand helical perturbation coil set on the centerstack, is also under consideration.

This material is based upon work supported by the U.S. Department of Energy, Office of Science, Office of Fusion Energy Sciences, under Award Number DE-FG02-96ER54375. Disclaimer: Any opinions, findings, and conclusions or recommendations expressed in this publication are those of the authors and do not necessarily reflect the views of the U.S. Department of Energy.

[1] GARSTKA, G D, et al., "The upgraded Pegasus Toroidal Experiment" Nucl. Fusion **46** (2006) S603-S612.

[2] THOME, K E, et al., "High Confinement Mode and Edge Localized Mode Characteristics in a near-unity aspect ratio tokamak", Phys. Rev. Lett. 116 (2016) 175001.

[3] BONGARD, M W, et al., "A Hall sensor array for internal current profile constraint" Rev. Sci. Instrum. **81** (2010) 10E105.

[4] SONTAG, A C, et al., "Equilibrium properties at very low aspect ratio in the Pegasus toroidal experiment" Nucl. Fusion **48** (2008) 095006.

[5] GROVER, F W, Inductance Calculations, D. Van Nostrand, New York, (1946).

[6] ROSA, E B, and Grover, F W, Formulas and tables for the calculation of mutual and self-inductance (Revised), Bulletin of the Bureau of Standards **8** (1912) 1.

[7] KIRK, A, et al., "Evolution of Filament Structures during Edge-Localized Modes in the MAST Tokamak", Phys. Rev. Lett. **96** (2006) 185001.

[8] SUGIYAMA, L E, "Mode coupling and aspect ratio effects on low and high- nplasma instabilities", Nucl. Fusion **55** (2015) 073006.

[9] PAMELA, S J P, et al., "Resistive MHD simulation of edge-localized-modes for double-null discharges in the MAST device", Plasma Phys. Control. Fusion, **55** (2013) 095001.

[10] SUGIYAMA, L E, "Intrinsic stochasticity in fusion plasmas", Phys. Scr., **86** (2012) 058205.

[11] GROEBNER, R J, and Osborne, T H, "Scaling studies of the high mode pedestal", Phys. Plasmas **5** (1998) 1800.

[12] MARTIN, Y R, TT T and Group I C H T D W, "Power requirement for accessing the H-mode in ITER", J. Phys.: Conf. Ser., **123** (2008) 012033.

[13] MAINGI, R, et al., "Overview of L–H power threshold studies in NSTX", Nucl. Fusion, **50 (**2010**)** 064010.

[14] WESSON, J, Tokamaks, Oxford University Press, Oxford (2004).

[15] MA, Y, et al., "Scaling of H-mode threshold power and L–H edge conditions with favourable ion grad-B drift in Alcator C-Mod tokamak", Nucl. Fusion, (2012).

[16] FUNDAMENSKI, W, Militello, F, Moulton, D, and McDonald, D, C, "A new model of the L–H transition in tokamaks", Nucl. Fusion, **52** (2012) 062003.

[17] BONGARD, M W, et al., "Characterization of peeling modes in a low aspect ratio tokamak"' Nucl. Fusion **54** (2014) 114008.

[18] MAINGI, R, et al., "Observation of a high performance operating regime with small edge-localized modes in the National Spherical Torus Experiment", Nucl. Fusion **45** (2005) 264-270.

[19] KASS, T, et al., "Characteristics of type I and type III ELM precursors in ASDEX upgrade, Nucl. Fusion, **38** (1998) 111-116.

[20] MAINGI, R, et al., "Edge-Localized-Mode Suppression through Density-Profile Modification with Lithium-Wall Coatings in the National Spherical Torus Experiment", Phys. Rev. Lett. **103** (2009) 075001.

[21] BONGARD, M W, et al., "Measurement of Peeling Mode Edge Current Profile Dynamics", Phys. Rev. Lett. **107** (2011) 035003.

[22] MYRA, J R, "Current carrying blob filaments and edge-localized-mode dynamics", Phys. Plasmas, **14** (2007) 102314.

[23] PAMELA, S J P, et al., "Nonlinear MHD simulations of edge-localized-modes in JET", Plasma Phys. Control. Fusion, **53 (**2011**)** 054014.

[24] BATTAGLIA, D J, et al., “Tokamak startup using outboard current injection on the Pegasus Toroidal Experiment”, Nucl. Fusion **51** (2011) 073029.

[25] JÜTTNER, B, “Cathode spots of electric arcs”, J. Phys. D: Appl. Phys., **34** (2001) R103-R123.

[26] SCHLOSSBERG, D J, et al., “A Thomson scattering diagnostic on the Pegasus Toroidal experiment”, Rev. Sci. Instrum. **83** (2012) 10E335.

[27] SCHOENBECK, N L, et al., “A compact multichannel spectrometer for Thomson scattering”, Rev. Sci. Instrum., **83** (2012) 10E330.

[28] SCHLOSSBERG, D J, et al., “Progress on Thomson scattering in the Pegasus Toroidal Experiment”, J. Inst., **8** (2013) C11019-C11019.

[29] O’BRYAN, J B, Sovinec, C R and Bird, T M, “Simulation of current-filament dynamics and relaxation in the Pegasus Spherical Tokamak”, Phys. Plasmas, **19** (2012) 080701-080701-4.

[30] O’BRYAN, J B, and Sovinec, C R, “Simulated flux-rope evolution during non-inductive startup in Pegasus”, iopscience.iop.org **56** (2014) 064005.

[31] BATTAGLIA, D J, et al., “Tokamak startup using outboard current injection on the Pegasus Toroidal Experiment”, Nucl. Fusion, **51** (2011) 073029.

[32] O’BRYAN, J B, Numerical Simulation of Non-Inductive Startup of the Pegasus Toroidal Experiment, C R Sovinec ed., (2014) Madison, WI.

[33] EIDIETIS, N W, et al., “Non-inductive Production of ST Plasmas with Washer Gun Sources on the Pegasus Toroidal Experiment”, J Fusion Energy, **26** (2007) 43-46.

[34] PEREZ, CP, et al., “Type-I ELM precursor modes in JET”, Nucl. Fusion **44** (2004) 609-623.